The application of a programmable servo controller to state control of an electrohydraulic active suspension

J Watton, K M Holford and P Surawattanawan

Proceedings of the Institution of Mechanical Engineers, Part D: Journal of Automobile Engineering 2004 218: 1367
DOI: 10.1243/0954407042707650

The application of a programmable servo controller to state control of an electrohydraulic active suspension

J Watton*, K M Holford and **P Surawattanawan**
Cardiff School of Engineering, Cardiff University, UK

Abstract: Fully active electrohydraulic control of a $\frac{1}{4}$ car test rig is considered from both a modelling and experimental point of view. Both pole assignment (PA) and linear quadratic control (LQC) techniques are used to design the state feedback gains with a view to achieving an optimum body acceleration characteristic, based on a validated linearized mathematical model. Computer simulation of the complete system suggests that the LQ control design approach gives the better performance characteristic. An industrial programmable servo controller (PSC) is implemented to drive two servo valves, one used for the road input actuator and the other used for the active control actuator. Programmable features are introduced, such as gain scheduling and state gain switching to achieve improved control. It is shown that although body displacement compensation is naturally achieved for road input changes, the global optimum design for acceleration transmissibility could not be achieved, due to practical limitations caused by the predicted low transducer gain between wheel and body. A further feature of the programmable controller approach was the ability to change state feedback gains during operation. This was found necessary to move the suspension from its initial rest position to its operating position. However, an improved performance in body acceleration amplitude control was still possible compared with the optimum passive suspension theoretical predictions.

Keywords: active suspension, modelling, electrohydraulic control

NOTATION

A	active actuator cross-sectional area $= 2.46 \times 10^{-4}$ m^2
$\mathbf{A}$	open-loop state space matrix
$\boldsymbol{B}$	open-loop state space vector
B_t	tyre damping $= 4000$ N/ms^{-1}
B_v	hydraulic cylinder and linkage damping $= 300$ N/ms^{-1}
$\mathbf{C}$	output state matrix
e	error signal
F	hydraulic force
$\boldsymbol{F_1}$	linear variable differential transducer (LVDT) gain $=$ 57.2 v/m
$\mathbf{F_2}$	feedback gain $= 1$
G	Moog 2000 program D/A gain $= 6.25 \times 10^{-3}$ mA/PSC no
$\boldsymbol{G_d}$	open-loop state space vector
i	servovalve current
i_0	steady state applied servo valve current
$\mathbf{I}$	identity matrix
$\boldsymbol{I_1}, \boldsymbol{J_1}, \boldsymbol{H_1}, \boldsymbol{F_1}, \boldsymbol{L_1}$	gain elements of the feedback vector
$\mathbf{I_2}, \mathbf{J_2}, \mathbf{H_2}, \mathbf{F_2}, \mathbf{L_2}$	transducer gain elements of the gain matrix
J	performance index for LQC
k_f	servovalve flow constant
k_i	linearized servo valve flow constant $= 2.3 \times 10^{-5}$ m^3 s^{-1}/mA
k_s	suspension stiffness range for the hypothetical passive suspension 20–118 kN/m
k_t	tyre stiffness $= 2.8 \times 10^5$ N/m
$\boldsymbol{K}$	state feedback gain vector
$\boldsymbol{K_1}$	state feedback gain vector
$\boldsymbol{K_2}$	transducer gain matrix
LQC	linear quadratic control
m	wheel and tyre mass (unsprung mass, $\frac{1}{4}$ car model) $= 40$ kg
M	car-body mass (sprung mass, $\frac{1}{4}$ car model) $= 240$ kg

The MS was received on 10 July 2003 and was accepted after revision for publication on 9 June 2004.
** Corresponding author: Cardiff School of Engineering, Cardiff University, Queens Buildings, The Parade, Cardiff, CF2 3TA, UK. email: watton@cardiff.ac.uk*

$\mathbf{M_C}$	open-loop system controllability matrix
N	Moog 2000 program A/D gain = 1600 PSC no/volt
P	forward gain for 2DOF test = 0.85
P_L	load pressure
$\mathbf{P_m}$	real symmetric matrix for LQC design
P_s	supply pressure
P_t	tank return pressure
P_1, P_2	pressures
P_{10}, P_{20}	steady state pressures
PA	pole assignment
PSC	programmable servo controller
q_i	elements of $\mathbf{Q_m}$
$\mathbf{Q_m}$	real symmetric matrix for LQC
Q_1, Q_2	flowrates
R	positive real number
R_i	cross-line leakage resistance = $9.8 \times 10^{10}\ \mathrm{Nm^{-2}/m^3\,s^{-1}}$
s	Laplace operator
$\mathbf{T}$	matrix for PA controller design
V	actuator and hose volume = $7.13 \times 10^{-5}\ \mathrm{m^3}$
$\mathbf{W_c}$	matrix for PA controller design
$\boldsymbol{x}$	open-loop state vector
y	system output
z_b	absolute displacement of the car body
$\dot{z}_b$	car-body (sprung mass) velocity
$\ddot{z}_b$	car-body (sprung mass) acceleration
z_r	absolute displacement of road disturbance
$\dot{z}_r$	velocity of road disturbance
z_{ref}	reference signal of z_b
z_w	absolute displacement of wheel (unsprung mass)
$\dot{z}_w$	wheel (unsprung mass) velocity
$\ddot{z}_w$	wheel (unsprung mass) acceleration
$z_b - z_w$	relative displacement of car body and wheel
$(z_b - z_w)_f$	feedback signal of $z_b - z_w$
$z_r - z_w$	relative displacement of road disturbance and wheel
α	actuator angle = 27°
β_e	effective bulk modulus = $0.22 \times 10^9\ \mathrm{M/m^2}$
ζ	damping ratio of the assumed control poles
ζ_p	damping ratio of the passive suspension second-order transfer function

1 INTRODUCTION

Supporting work to this study considered the mathematical modelling and parameter identification of an active suspension test facility, as shown in Figs 1 and 2. The test rig is a TVR suspension and wheel unit with a Lotus active suspension actuator with integral position sensor, and is fully instrumented to measure all positions, accelerations, and applied force. In addition, the dynamic performance of the active actuator may be analysed from the dynamic signals generated by pressure transducers and fast-acting flow meters placed in the two lines between the servo valve and actuator. The digital control system employs two 2-channel Moog M2000 programmable servo controllers (PSCs), one connected to the Lotus actuator and the other to the road input actuator [**1**, **2**]. An additional data acquisition system is also available to log the system dynamic behaviour.

There have been many studies on vehicle suspension systems, some containing a substantial number of references [**3**–**6**], but those considering electrohydraulic solutions tend to overlook detailed hydraulic modelling. Further work has considered theoretical simulations employing various simplifications and/or neglect of hydraulic characteristics, such as bulk modulus, actuator leakage, servo valve gain changes when raising or lowering, actuator equivalent transfer function, and various combinations of these. However, it is clear that the inclusion of these various effects leads to a complicated overall model, particularly when control design rules need to be established [**7**–**14**]. Outcomes are difficult to compare, since there are many different actuation techniques, and hence mathematical models, used with

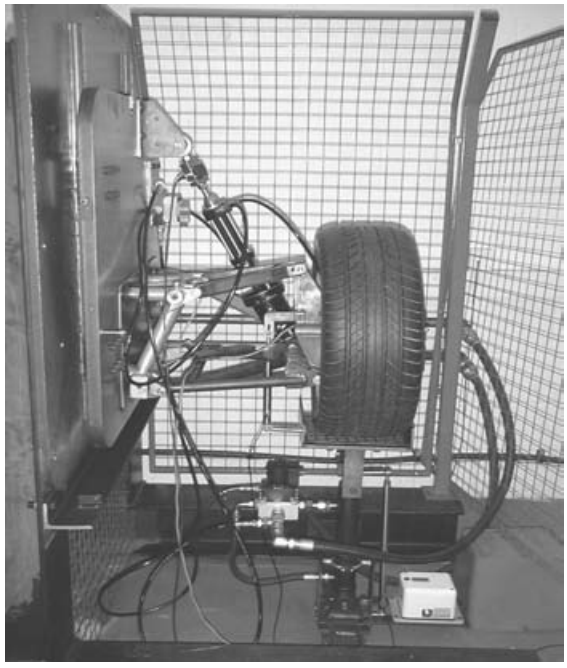

Fig. 1 Photograph of the test rig

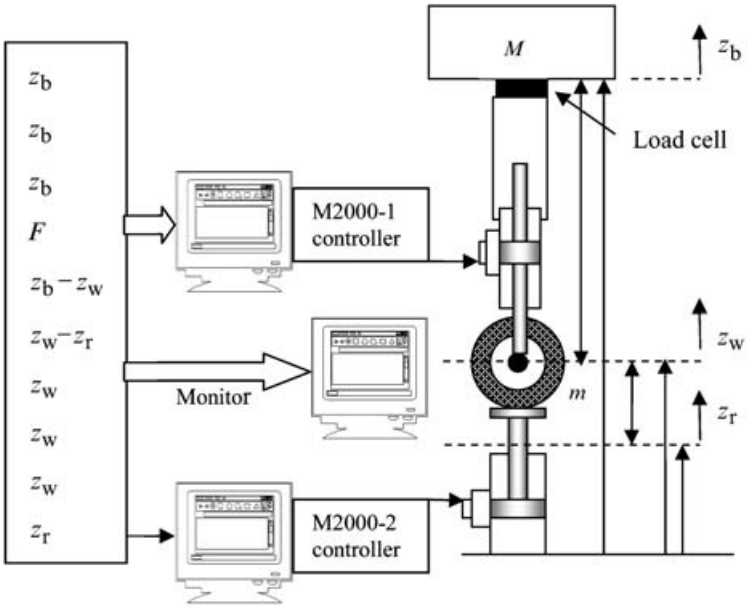

Fig. 2 Schematic of the experimental test rig

limited experimental evidence to validate the models assumed. The significance of servovalve non-linear flow characteristics is well established, although the effect of changing flow gains is difficult to address theoretically for control design purposes. Unless some attempt is made to do this experimentally in the hardware control loop, as is the case for this study, it is difficult to justify a linearized analysis approach [**1**, **2**]. This related work has also shown that the dynamics of the actuator have a significant effect on the system transfer function model, with actuator damping due to leakage being a key factor. In terms of control law selection in the presence of hydraulic effects, combinations of state variables, including force, have been used to select linear control laws. Linear quadratic control (LQC) has been considered using force control [**8**, **11**] via simulation using simplified mathematical models for the actuator. Adaptive observers have also been considered using the same state variables as this study [**10**], although, as with the LQC approaches, suspension stiffness was present in parallel with the active actuator.

2 System open-loop performance and control approach

Considering earlier work [**1**, **2**], a system modelling and control approach was outlined, including detailed hydraulic dynamic effects. Various submodels were validated experimentally and it was shown that the active suspension performance could be adequately modelled, and potentially controlled, using five measured states. Considering the system equations given in the Appendix, the state space approach shown in Table 1 is developed.

It was shown that the open-loop equations may be written in the following state space format

$$\dot{\boldsymbol{x}} = \mathbf{A}\boldsymbol{x} + \boldsymbol{B}e + \boldsymbol{G_d}\dot{z}_r \tag{1}$$

$$\boldsymbol{x} = \begin{bmatrix} \dot{z}_b \\ \dot{z}_w \\ F \\ z_b - z_w \\ z_w - z_r \end{bmatrix}$$

$$\mathbf{A} = \begin{bmatrix} -\dfrac{B_v}{M} & \dfrac{B_v}{M} & \dfrac{\cos\alpha}{M} & 0 & 0 \\ \dfrac{B_v}{m} & -\dfrac{(B_v + B_t)}{m} & -\dfrac{\cos\alpha}{m} & 0 & -\dfrac{k_t}{m} \\ -\dfrac{2\beta_e A^2}{V} & \dfrac{2\beta_e A^2}{V} & -\dfrac{2\beta_e}{VR_i} & 0 & 0 \\ 1 & -1 & 0 & 0 & 0 \\ 0 & 1 & 0 & 0 & 0 \end{bmatrix}$$

$$\boldsymbol{B} = \begin{bmatrix} 0 \\ 0 \\ \dfrac{2k_i AGP\beta_e}{V} \\ 0 \\ 0 \end{bmatrix} \qquad \boldsymbol{G_d} = \begin{bmatrix} 0 \\ \dfrac{B_t}{m} \\ 0 \\ 0 \\ -1 \end{bmatrix} \tag{2}$$

Table 1 State notation

Measurement	State variable
Car body velocity, $\dot{z}_b$	x_1
Wheel hub velocity, $\dot{z}_w$	x_2
Hydraulic force, F	x_3
Suspension displacement, $z_b - z_w$	x_4
Tyre deflection, $z_w - z_r$	x_5

As shown in Fig. 2, control is based around the Moog M2000 digital programmable servo controller (PSC). Two units were used, with each unit capable of controlling two servovalves. Key features of the PSC are:

1. The Engineering User Interface is a text-based programming language specifically designed for the configuration and programming of the PSC. The software is installed in each of the supervisory PCs and runs automatically when the computers are switched on.
2. Programs are created off-line using ASCII code called a 'log file'. When a program is loaded, it is automatically compiled (alerting the user of any errors) and transferred to the PSC via the RS232 serial link.
3. The program continues to run until either the computer is switched off or another program is loaded.
4. While the PSC is running a program, the operator is presented with a screen displaying key system parameters. The screen is split into two with a maximum of 16 parameters displayed on the left-hand side, which can be modified, and up to a further 16 parameters on the right-hand side for real-time monitoring.

The most suitable control approach, via either pole assignment (PA) or linear quadratic control (LQC), will first be determined by computer simulation. This is done to minimize control loop instability of the test rig by random selection of individual transducer gains. A diagram of the modelling and state control approach is shown in Fig. 3.

One novel feature of the PSC approach is the ability to gain schedule the servo valve control signal. This effectively compensates for the effect of servo valve flow gain change depending on whether the active actuator is extending or retracting. This effect is significant and the implementation of gain scheduling has two advantages:

1. The transient response in either direction may be matched within the constraints of the practical limitation, due principally to dynamic pressure differential change effects.
2. The linearized dynamic model may be used with more confidence since it assumes constant servo valve flow gains in each direction.

It can be shown that by assuming a mean load equivalent to the body mass effect the ratio of gains is given by [**1**]

$$\frac{\text{Gain retracting}}{\text{Gain extending}} = \frac{\sqrt{P_s + \dfrac{Mg}{A}}}{\sqrt{P_s - \dfrac{Mg}{A}}} = 1.69 \tag{3}$$

The gain may be apportioned in a number of ways, typically one increasing by a factor of 1.3 and the other decreasing by the same factor. Validation between measurement and linearized theory, with gain compensation, is given in [**1**, **2**].

For state control, the control signal is e and the disturbance signal is $\dot{z}_r$, the velocity of the road

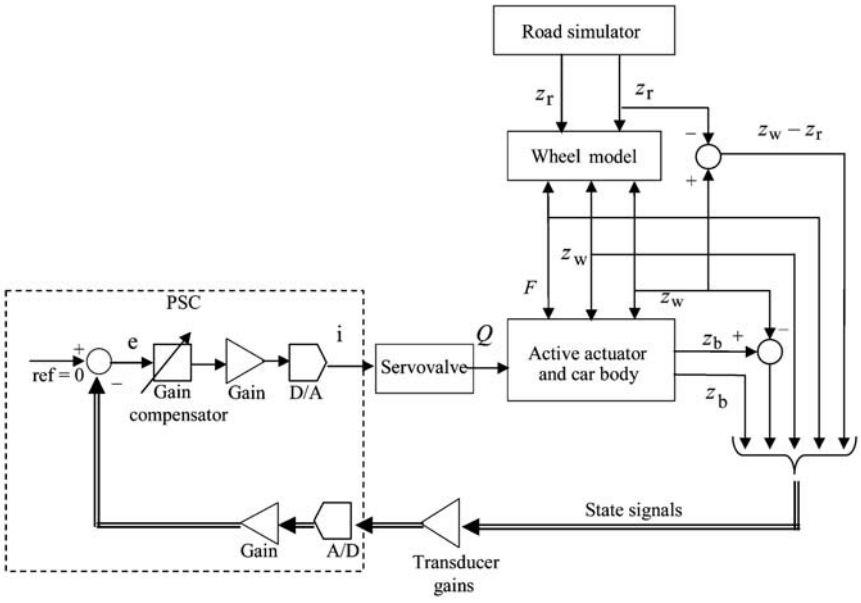

Fig. 3 Simulation and control concept

disturbance. For state feedback, and considering the implementation of the Moog M2000 PSC, the control signal is given by

$$e = -\boldsymbol{K}\boldsymbol{x} = -N\boldsymbol{K}_1\mathbf{K}_2\boldsymbol{x}$$

$$e = -N[\boldsymbol{I}_1\mathbf{I}_2\dot{z}_b + \boldsymbol{J}_1\mathbf{J}_2\dot{z}_w + \boldsymbol{H}_1\mathbf{H}_2F + \boldsymbol{F}_1\mathbf{F}_2(z_b - z_w) = \boldsymbol{L}_1\mathbf{L}_2(z_w - z_r)] \tag{4}$$

$\boldsymbol{K}_1$ = state feedback gain vector for the controller

$$= [\boldsymbol{I}_1 \quad \boldsymbol{J}_1 \quad \boldsymbol{H}_1 \quad \boldsymbol{F}_1 \quad \boldsymbol{L}_1]$$

$\mathbf{K}_2$ = known transducer gain matrix

$$\begin{bmatrix} \mathbf{I}_2 & 0 & 0 & 0 & 0 \\ 0 & \mathbf{J}_2 & 0 & 0 & 0 \\ 0 & 0 & \mathbf{H}_2 & 0 & 0 \\ 0 & 0 & 0 & \mathbf{F}_2 & 0 \\ 0 & 0 & 0 & 0 & \mathbf{L}_2 \end{bmatrix} \tag{5}$$

3 CONTROLLER DESIGN USING THE POLE ASSIGNMENT (PA) METHOD

This study considers both PA and linear quadratic optimal control methods for controller design selection. Considering first PA and performing some preliminary calculations, using the data given previously, shows that

$$\mathbf{A} = \begin{bmatrix} -1.25 & 1.25 & 3.71\times10^{-3} & 0 & 0 \\ 7.5 & -1.08\times10^{2} & -2.22\times10^{-2} & 0 & -7\times10^{3} \\ -3.73\times10^{5} & 3.73\times10^{5} & -63 & 0 & 0 \\ 1 & -1 & 0 & 0 & 0 \\ 0 & 1 & 0 & 0 & 0 \end{bmatrix}$$

$$\boldsymbol{B} = \begin{bmatrix} 0 \\ 0 \\ 186 \\ 0 \\ 0 \end{bmatrix} \tag{6}$$

The controllability matrix is written

$$\mathbf{M}_c = [\boldsymbol{B} \quad \mathbf{A}\boldsymbol{B} \quad \mathbf{A}^2\boldsymbol{B} \quad \mathbf{A}^3\boldsymbol{B} \quad \mathbf{A}^4\boldsymbol{B}] \tag{7}$$

The rank of $\mathbf{M}_c$ is 5 and the system is state controllable. The open-loop characteristic equation is

$$|s\mathbf{I} - \mathbf{A}| = a_0 + a_1 s + a_2 s^2 + a_3 s^3 + a_4 s^4 + a_5 s^5 \tag{8}$$

and a desired closed-loop characteristic equation is

$$\alpha_0 + \alpha_1 s + \alpha_2 s^2 + \alpha_3 s^3 + \alpha_4 s^4 + \alpha_5 s^5 \tag{9}$$

The solution for the feedback signal is then given by

$$e = -\boldsymbol{K}\boldsymbol{x}$$

$$\boldsymbol{K} = [\alpha_0 - a_0 \quad \alpha_1 - a_1 \quad \alpha_2 - a_2 \quad \alpha_3 - a_3 \quad \alpha_4 - a_4]\mathbf{T}^{-1}$$

$$\mathbf{T} = \mathbf{M}_c\mathbf{W}_c$$

$$\mathbf{W}_c = \begin{bmatrix} a_1 & a_2 & a_3 & a_4 & 1 \\ a_2 & a_3 & a_4 & 1 & 0 \\ a_3 & a_4 & 1 & 0 & 0 \\ a_4 & 1 & 0 & 0 & 0 \\ 1 & 0 & 0 & 0 & 0 \end{bmatrix}$$

$$= \begin{bmatrix} 1.02\times10^{7} & 5.96\times10^{5} & 2.37\times10^{4} & 1.72\times10^{2} & 1 \\ 5.96\times10^{5} & 2.37\times10^{4} & 1.72\times10^{2} & 1 & 0 \\ 2.37\times10^{4} & 1.72\times10^{2} & 1 & 0 & 0 \\ 1.72\times10^{2} & 1 & 0 & 0 & 0 \\ 1 & 0 & 0 & 0 & 0 \end{bmatrix}$$

$$\mathbf{T} = \begin{bmatrix} 7.55\times10^{-10} & 4.82\times10^{3} & 68.8 & 0.688 & 0 \\ -9.22\times10^{-9} & 1.58\times10^{-11} & 4.69\times10^{-13} & -4.13 & 0 \\ -1.24\times10^{-5} & 1.62\times10^{6} & 1.32\times10^{6} & 2.02\times10^{4} & 186 \\ 4.82\times10^{3} & 68.8 & 4.82 & 0 & 0 \\ 1.58\times10^{-11} & 4.69\times10^{-13} & -4.13 & 0 & 0 \end{bmatrix} \tag{10}$$

As a design start, the two dominant poles were selected to be $-7.45 \pm 6.37j$, giving an undamped natural frequency of 1.56 Hz and a damping ratio of 0.76, the three remaining closed-loop poles being placed at -74.5. As will be shown later, this pole selection gives a solution for the state controller that is at the optimum condition to minimize body acceleration, as predicted from the simulation study. The solution then becomes

$$\boldsymbol{K} = [-756 \quad 2500 \quad 0.359 \quad 8250 \quad 91\,000] \tag{11}$$

from equation (3)

$$\boldsymbol{K}_1 = N^{-1}\boldsymbol{K}\mathbf{K}_2^{-1}$$

$$\mathbf{K}_2 = \begin{bmatrix} 5 & 0 & 0 & 0 & 0 \\ 0 & 5 & 0 & 0 & 0 \\ 0 & 0 & 66.7\times10^{-6} & 0 & 0 \\ 0 & 0 & 0 & 57.2 & 0 \\ 0 & 0 & 0 & 0 & 18.2 \end{bmatrix}$$

$$\boldsymbol{K}_1 = [-0.0944 \quad 0.313 \quad 3.37 \quad 0.09 \quad 3.13] \tag{12}$$

4 CONTROLLER DESIGN USING LINEAR QUADRATIC OPTIMAL CONTROL

The theory of LQC is well established [2, 8, 11, 15], although it does not appear to have been applied to an active suspension modelled to the hydraulic detail appropriate to this study. The performance index used is given by

$$J = \int_0^\infty (y^{\mathrm{T}}\mathbf{Q}_{\mathbf{m}}y + e^{\mathrm{T}}Re)\mathrm{d}t \qquad \mathbf{Q}_{\mathbf{m}} = \begin{bmatrix} q_1 & 0 & 0 \\ 0 & q_2 & 0 \\ 0 & 0 & q_3 \end{bmatrix}$$

and assuming $y = \mathbf{C}\boldsymbol{x}$

$$\mathbf{C} = \begin{bmatrix} 0 & 0 & 1 & 0 & 0 \\ 0 & 0 & 0 & 1 & 0 \\ 0 & 0 & 0 & 0 & 1 \end{bmatrix}$$

$$J = \int_0^\infty (\boldsymbol{x}^{\mathrm{T}}\mathbf{C}^{\mathrm{T}}\mathbf{Q}_{\mathbf{m}}\mathbf{C}\boldsymbol{x} + \boldsymbol{x}^{\mathrm{T}}\boldsymbol{K}^{\mathrm{T}}R\boldsymbol{K}\boldsymbol{x})\mathrm{d}t \tag{13}$$

The gain matrix in this case is obtained via solution of the reduced matrix Ricatti equation to initially determine the symmetric matrix, $\mathbf{P}_{\mathbf{m}}$

$$\mathbf{A}^{\mathrm{T}}\mathbf{P}_{\mathbf{m}} + \mathbf{P}_{\mathbf{m}}\mathbf{A} + \mathbf{C}^{\mathrm{T}}\mathbf{Q}_{\mathbf{m}}\mathbf{C} - \mathbf{P}_{\mathbf{m}}^{\mathrm{T}}\boldsymbol{B}R^{-1}\boldsymbol{B}^{\mathrm{T}}\mathbf{P}_{\mathbf{m}} = 0 \tag{14}$$

For this study $\mathbf{P}_{\mathbf{m}}$ contains 15 constants that are determined from equation (14). The state feedback gain, $\boldsymbol{K}_1$, is then determined from

$$\boldsymbol{K} = R^{-1}\boldsymbol{B}^{\mathrm{T}}\mathbf{P}_{\mathbf{m}} \qquad \boldsymbol{K}_1 = N^{-1}\boldsymbol{K}\mathbf{K}_2^{-1} \tag{15}$$

The difficult aspect of this approach is the selection of the four weighting parameters, R, q_1, q_2, and q_3. Recalling previous work [**2**, **15**] the global minimum point determination is not affected by the choice of R, which is selected to have a value $R = 1$. Since q_2 and q_3 vary with the square of the measured variables $(z_{\mathrm{b}} - z_{\mathrm{w}})$ and $(z_{\mathrm{w}} - z_{\mathrm{r}})$, then it is proposed that the ratio q_3/q_2 is also specified as a square law, evaluated using each maximum displacement: in this study 25 mm and 6.6 mm. Hence, $q_3/q_2 = 13.5$ and the problem is reduced to selecting just q_1 and q_2. As a design start, then selecting $q_1 = 43.7$ and $q_2 = 2 \times 10^6$ gives

$$\boldsymbol{K} = [-420 \quad 1690 \quad 6.25 \quad 1410 \quad -8100]$$

$$\boldsymbol{K}_1 = [-0.053 \quad 0.211 \quad 58.5 \quad 0.015 \quad -0.278] \tag{16}$$

5 CONTROLLER SELECTION VIA COMPUTER SIMULATION

Following the establishment of ostensibly workable control laws, using both PA and LQC methods, the active control performance may be further evaluated via computer modelling; in this study within the Matlab Simulink environment. In practice this means a large number of simulations, selected as 150 for this study, as the following parameters are varied:

1. The undamped natural frequency and damping ratio for PA control.
2. The weighting factors q_1 and q_2 for LQC.

A random road input model was used and the r.m.s. values of the appropriate system variable was used to compare results. An integrator with a gain of 0.223 was used to represent the transfer function relating the road input displacement to Gaussian white noise representing the road input velocity. The gain represents the situation when a vehicle runs at a relatively high speed of 150 km/hr on a relatively rough road surface, and a simulation time of 40 s was used for all simulations. Therefore, the average level of the road input displacement changes with time and is considered to be representative of a real road surface.

For completeness, it is useful to compare the purely passive suspension and this is done by assuming typical, yet hypothetical for this study, suspension stiffnesses in the range $k_{\mathrm{s}} = 20$–118 kN/m. A suspension damping rate is implied by assuming the equivalent damping ratio of the resulting second-order transfer function for the suspension mode of vibration. Hence, a complete plot of body r.m.s. acceleration may be obtained, as discussed previously, and the result is shown in Fig. 4. For all the simulation results shown in Figs 4, 5, and 6 the maximum r.m.s. values are $(z_{\mathrm{w}} - z_{\mathrm{b}})$ maximum = 25 mm and $(z_{\mathrm{r}} - z_{\mathrm{w}})$ maximum = 6.8 mm. Results for the r.m.s. acceleration of the vehicle body are shown in Fig. 5 for PA control and Fig. 6 for LQC.

Comparing the two sets of control results shown in Figs 5 and 6, shows that the linear quadratic design

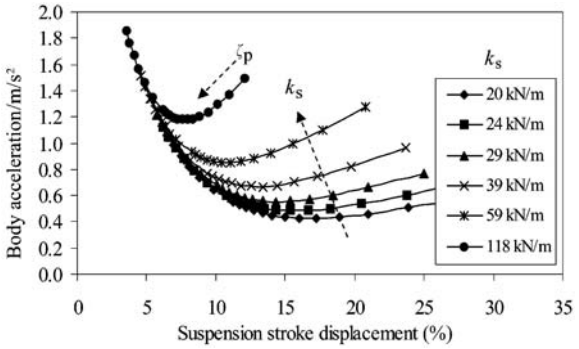

Fig. 4 Body r.m.s. acceleration for road test random input profile, passive suspension

Table 2 Optimum performance comparisons for the three suspension designs

System variable	Passive suspension	Pole assignment (PA) control	Linear quadratic (LQ) control
Body acceleration $\ddot{z}_b$ m/s^2	0.43	0.22	0.12
Suspension displacement $z_w - z_b$ % maximum value	17	15	24
Tyre deflection $z_r - z_w$ % maximum value	10	10	10
Applied current to servovalve **I** % maximum value	Not applicable	2.2	2.3

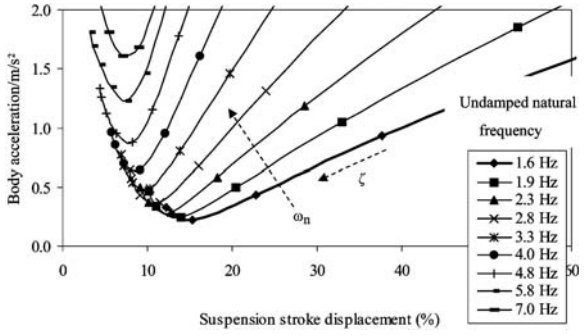

Fig. 5 Body r.m.s. acceleration for road test random input profile, PA control

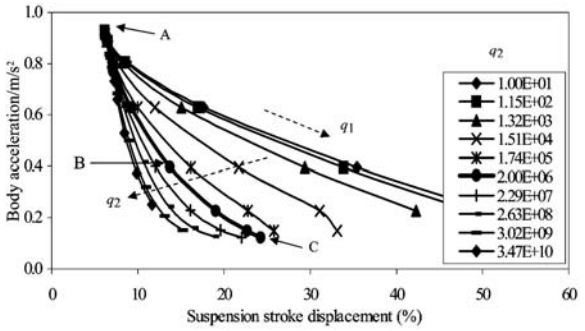

Fig. 6 Body r.m.s. acceleration for road test random input profile, LQC

approach can potentially offer a greater reduction in r.m.s. acceleration. Reducing the undamped natural frequency below 1.56 Hz for PA control has little effect on the global minimum. For LQC, large changes in both q_1 and q_2 are required to produce a small change in the global minimum. In fact this point becomes relatively insensitive to such changes. For the purpose of control selection the estimated global minimum conditions are compared in Table 2, which also includes the passive suspension results.

It can be seen from Table 2 that LQC produces the better performance in terms of minimizing the r.m.s. acceleration. The level is reduced to 28 per cent of the optimum passive suspension value and to 55 per cent of the optimum PA value. However, this is at the expense of an increased suspension displacement and a negligible increase in servo valve current.

It is next convenient to consider a frequency response analysis of the results since this provides a further comparison for road surfaces with repetitive wheel excitations. It also allows a more meaningful comparison of the transfer functions previously developed [**1**, **2**]. Figure 7 shows the dominant poles for each optimum condition and Table 3 compares the resulting dynamic characteristics of the system for each optimum condition. In reality all the three conditions are representative of a second order transfer function, the linear quadratic solution being heavily damped due to the dominant real poles shown in Fig. 7.

It can be seen that optimum passive suspension design results in very low damping, the PA design has a more satisfactory damping ratio, and the LQ design

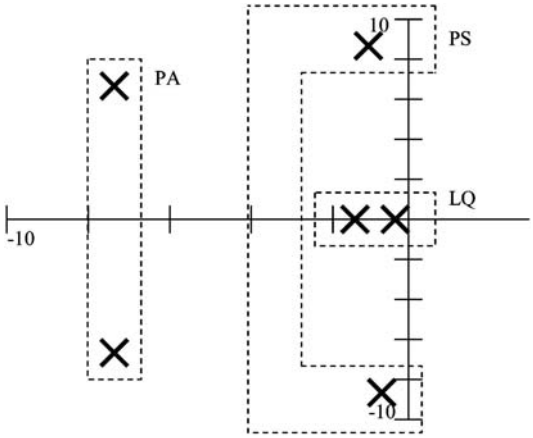

Fig. 7 Location of the dominant poles for each of the optimum designs

Table 3 The dominant second order transfer functions for each optimum design

Parameter	Passive suspension	PA control	LQC
Dominant natural frequency (Hz)	1.4	1.56	0.08
Damping ratio ζ	0.15	0.76	1

is critically damped suggesting a preferred operating characteristic. To obtain a more complete picture of the frequency characteristic, a comparison is now made by considering the complete transfer function for a range of designs around the optimum. Figure 8(a) shows the results for the passive suspension where the suspension damping is varied, Fig. 8(b) shows the results for PA control where the dominant damping ratio is varied, and Fig. 8(c) shows the results for LQC where one of the weighting parameters is varied.

The passive suspension result shows that a significant variation in the damping ratio from the optimum is required to avoid oscillations in acceleration amplitude response at the resonant frequencies of 1.4 Hz and 13.6 Hz. As the damping ratio is decreased this is equivalent to moving in an anticlockwise direction around the optimum curve shown in Fig. 4. Figure 8(a) shows a good reduction in acceleration transmissibility at higher frequencies, but at the expense of oscillations at the body natural frequency of 1.4 Hz. PA control is shown to produce a transmissibility that is sensitive to changes around the proposed optimum condition. As with the passive suspension, a decrease in the damping ratio is equivalent to moving in an anticlockwise direction around the optimum curve shown in Fig. 5. In general the transmissibility is increased as damping is changed either side of the optimum setting.

Since in practice a compromise in gain settings is inevitably required, this suggests that PA control is not the preferred approach. Figure 8(c) shows a more robust approach using LQC. Decreasing the weighting constant, q_1, means moving up the optimum condition curve shown in Fig. 6, and this monotonically increases the transmissibility. Figure 8(c) illustrates large reductions in q_1 and the results show a more robust LQC design compared with the PA controller design. The theoretical results for the LQC design suggest a low undamped natural frequency, as shown in Table 3, but the damping ratio is increased to a critical value and allows a reduction in car body acceleration over a wide frequency range. It was also shown in Table 2 that each optimum scheme indicated no difference in the tyre deflection or the control current used in the case of feedback only. LQC was therefore selected for the practical evaluation.

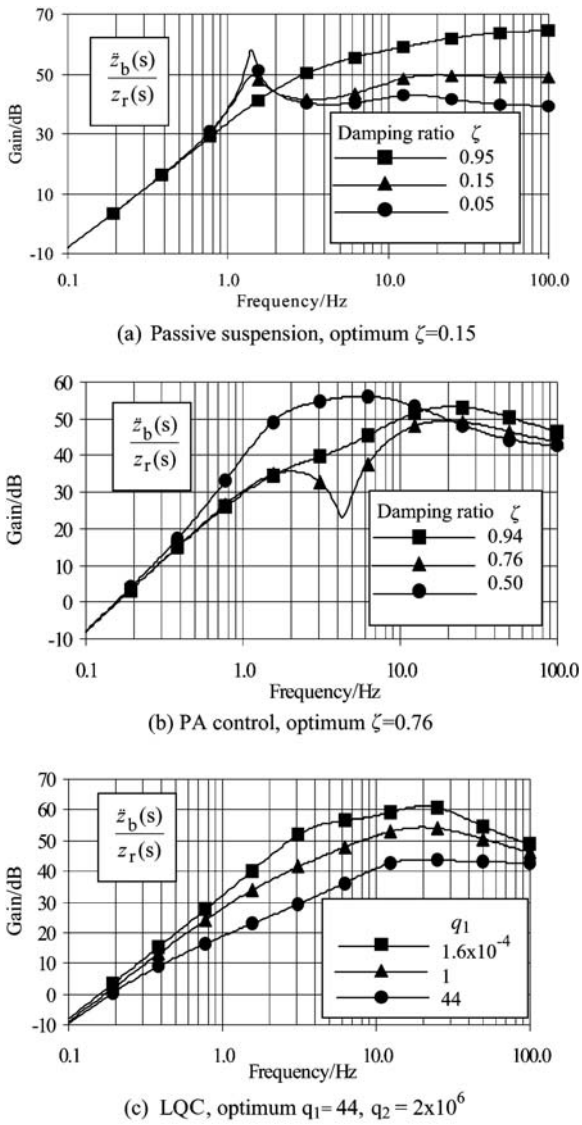

Fig. 8 Amplitude response for variations around the optimum design

6 EXPERIMENTAL VALIDATION OF THE PRFERRED LQ CONTROLLER

Both optimum PA and LQC designs result in extremely low feedback gains for the body-to-wheel ($z_w - z_b$ in practice) displacement transducer, as evident from the calculations shown in equations (12) and (16). The design is also limited to the mid-position of the active actuator since this is the condition about which the open-loop hydraulic linearized model is based. However, when the system is shut down the active actuator naturally moves to its fully retracted position, due to the body mass combined with hydraulic leakage. These combined aspects means that for the preferred closed-loop operating condition the initial servovalve current is insufficient to move the body from its rest position to the operating mid-position following subsequent start up of the system. Fortunately, a further novel feature of the Moog PSC is the ability to switch gains in real time, thus allowing different settings to be used for both rest and operating conditions. Before this gain switching is done it is preferable to consider its implication from a theoretical point of view.

Consider Fig. 6 and the trajectory containing the optimum condition, as indicated via the path A–B–C. None of these conditions allowed initial positioning of the suspension for the reason previously stated, and it was concluded that the theoretical optimum given by

$q_1 = 44$ and $q_2 = 2 \times 10^6$ could not be implemented. Moving to the left-hand side of the mapping shown in Fig. 6 reduces the suspension stroke displacement, for example selecting $q_2 = 3 \times 10^9$ reduces the maximum stroke displacement by $\frac{1}{3}$. Moving down the trajectory via similar points A–B–C as before means that the dominant closed-loop poles move off the negative real axis in the s plane such that the natural frequencies vary between 2.9 and 0.88 Hz with a damping ratio change from 0.65 to 0.72. Thus it can be seen that increasing the penalty function for $z_w - z_b$ causes a degradation in the acceleration isolation performance. However, under this new trajectory it was found possible to move the active actuator to its mid-position after control is initiated, although points A to B were only experimentally viable.

Comparisons between theory and experiment were then made by selecting $q_2 = 3 \times 10^9$ with an initial value of $q_1 = 2 \times 10^{-4}$ to determine the gain settings. With the system now operating with the active actuator in its mid-position, and for a sinusoidal road input, the new gains were calculated using $q_1 = 1$, the maximum viable, and then switched. An accelerometer was attached to the body and the effect of this gain change at a frequency of 5 Hz is shown in Fig. 9.

It is clear from Fig. 9 that the gain switch is stable and significantly reduces the vibration amplitude. Similar results were obtained at lower frequencies and a comparison between simulation and measurement is shown in Figs 10 and 11.

Measured signal distortion is observed from Figs 10 and 11, primarily due to the fact that the road input actuator is of the single-rod type and the servo valve control characteristic does not have gain scheduling. Hence, a sinusoidal signal to the servovalve does not result in a symmetrical sinusoidal road actuator motion. However, the results are sufficient to validate that state feedback gain changes along a chosen trajectory do improve the acceleration amplitude although movement to a region close to the global minimum is not practically possible. It does seem for the conditions studied under LQC, the acceleration amplitude reduction is of the order of 30 percent compared with the passive suspension global minimum condition. The latter of course has no body displacement correction for road input changes.

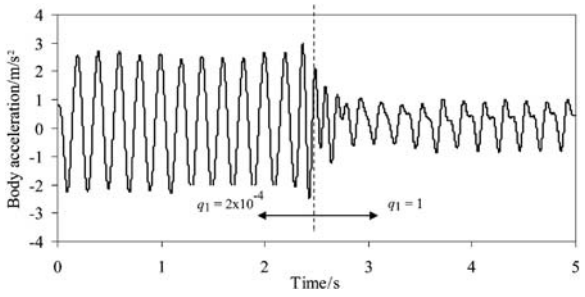

Fig. 9 Effect of state feedback gain changes for non-optimal conditions, $q_2 = 3 \times 10^9$, 5 Hz

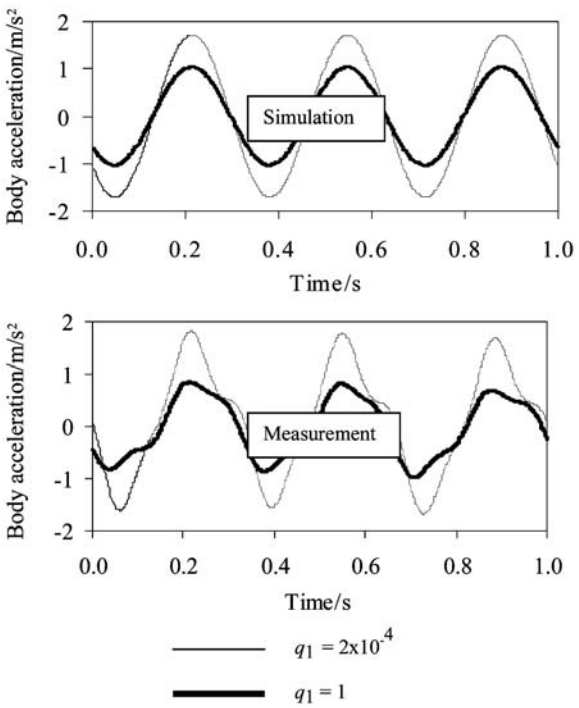

Fig. 10 Body acceleration for LQC at a frequency of 3 Hz

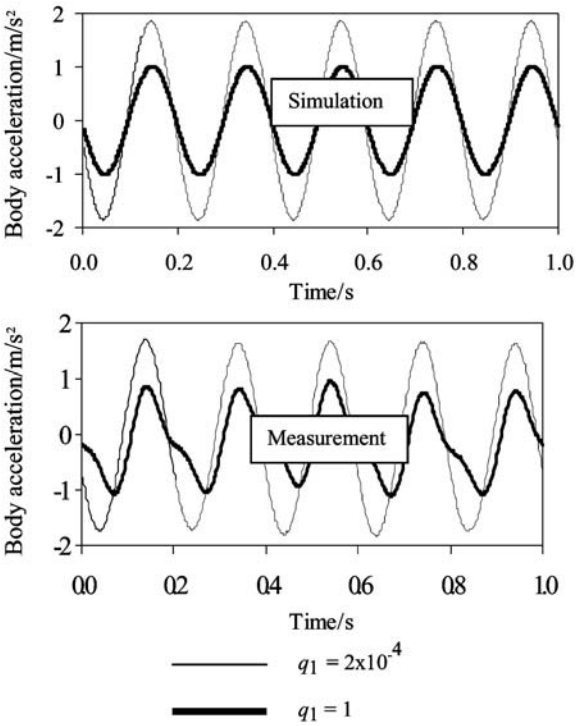

Fig. 11 Body acceleration for LQC at a frequency of 5 Hz

For the damped passive suspension design that must exist away from the global minimum condition, as shown in Fig. 8(a), the modified linear quadratic design would give an acceleration amplitude reduction of, typically, 78 percent over the frequency range shown.

7 CONCLUSIONS

The LQC design approach was found to be better than the PA approach since it effectively shifts the dominant natural frequency to a lower value. This leads to a 'softer' control approach and allows the damping rate to be increased to near its critical value. The linear quadratic approach has a greater flexibility since it allows different weights to be assigned to each measured state.

It was found that a great deal of experience was needed to select the linear quadratic design weights and following many analytical solutions to the matrix Ricatti equation, a global minimum point could be theoretically established. This resulted in a very low suspension position gain to the extent that the suspension could not be moved from its rest position to its operating mid-position. It is concluded that the complex system mathematical model, due to the inclusion of practical hydraulic characteristics, means that only suboptimal solutions are possible.

The theoretical design approaches considered were considerably aided by the ability to gain schedule the servo valve gain in practice, allowing a linearized theory to be more applicable to the open-loop non-linear equations. The programming facility of the PSC was also particularly useful in selecting different state feedback gains to allow the suspension to be moved to its operating position.

REFERENCES

1 **Watton, J., Holford, K. M.** and **Surawattanawan, P.** Electrohydraulic effects on the modelling of a vehicle active suspension, *Proc. Instn Mech. Engrs, Part I: Systems and Control Engineering*, 2001, **215**, 1077–1092.

2 **Surawattanawan, P.** The influence of hydraulic system dynamics on the behaviour of a vehicle active suspension, PhD Thesis, School of Engineering, Cardiff University, 2000.

3 **Sharp, R. S.** and **Crolla, D. A.** Road vehicle suspension system design: a review, *Veh. Sys. Dyn.*, 1987, **16**, 167–192.

4 **Appleyard, M.** and **Wellstead, P. E.** Active suspensions: some background, *IEE Proc., Part D: Control Theory Appl.*, 1995, **142**, 123–12.

5 **Elbeheiry, E. D.** ***et al.*** Advanced ground vehicle suspension systems: a classified bibliography, *Veh. Sys. Dyn.*, 1995, **24**, 231–258.

6 **Hrovat, D.** Survey of advanced suspension developments and related optimal control applications, *Automatica*, 1997, **33**, 1781–1817.

7 **Mrad, R. B.** ***et al.*** A nonlinear model of an automobile hydraulic active suspension, *ASME Adv. Automat. Technol.*, 1991, **40**(DE), 347–359.

8 **Engelmann, G. H.** and **Rizzoni, G.** Including the force generation process in active suspension control formulation. In Proceedings of the American Control Conference, San Francisco, USA, 1993, 701–705.

9 **Rajamani, R.** and **Hedrick, J. K.** Performance of active automotive suspensions with hydraulic actuators: theory and experiment. In Proceedings of the American Control Conference, 1994, 1214–1218.

10 **Rajamani, R.** and **Hedrick, J. K.** Adaptive observers for active automative suspensions: theory and experiment, *IEEE Trans. Control Sys. Technol.*, 1995, **3**(1), 86–93.

11 **Thompson, A. G.** and **Chaplin, P. M.** Force control in electrohydraulic active suspensions, *Veh. Sys. Dyn.*, 1996, **25**, 185–202.

12 **Williams, R. A.** Automotive active suspensions, part 1: basic principles, *Proc. Instn Mech. Engrs, Part D: J. Automobile Engineering*, 1997, **211**, 415–426.

13 **Williams, R. A.** Automotive active suspensions, part 2: practical considerations, *Proc. Instn Mech. Engrs, Part D: J. Automobile Engineering*, 1997, **211**, 427–444.

14 **Purdy, D. J.** and **Bulman, D. N.** An experimental and theoretical investigation into the design of an active suspension system for a racing car, *Proc. Instn Mech. Engrs, Part D: J. Automobile Engineering*, 1997, **211**, 161–173.

15 **Thomson, A. G.** An active suspension with optimal state feedback, *Veh. Sys. Dyn.*, 1976, **5**, 187–203.

APPENDIX: SYSTEM EQUATIONS

Following experimental flow measurements on the servo-valve [**18**], the non-linear servo valve flowrate equations are modelled as follows

For $i \geqslant 0$ when extending

$$Q_1 = k_f i \sqrt{|P_s - P_1|}\ \text{sign}\,(P_s - P_1)$$
$$Q_2 = k_f i \sqrt{P_2} \tag{17}$$

For $i < 0$ when retracting

$$Q_1 = k_f i \sqrt{P_1}$$
$$Q_2 = k_f i \sqrt{|P_s - P_2|}\ \text{sign}\,(P_s - P_2) \tag{18}$$

To obtain the equivalent linearized dynamic transfer functions for the system, we note the steady-state condition $i_0 = 0$, $P_1 = P_{10}$, $P_2 = P_{20}$, and the flowrate equations become

$$Q_1 = Q_2 = k_i i \tag{19}$$

where the flow gain, k_i, is as follows

$$k_i = k_f \sqrt{\frac{P_s - P_L}{2}} \text{ when extending}$$
$$\text{and } k_f \sqrt{\frac{P_s + P_L}{2}} \text{ when retracting} \tag{20}$$

$$P_L = P_{10} - P_{20} = Mg/A \tag{21}$$

As indicated by equation (3) the real-time adaption of flow gain via the Moog PSC means that for the subsequent analysis, equal extending and retracting flow gains may be used

$$k_i = k_f \sqrt{\frac{P_s + P_L}{2}} \Big/ 1.3 \tag{22}$$

The actuator flowrate equations, including compressibility and cross-line leakage effects, may be written

$$Q_1 = A(\dot{z}_b - \dot{z}_w) + \frac{V}{\beta_e}\dot{P}_1 + \frac{(P_1 - P_2)}{R_i} \tag{23}$$

$$Q_2 = A(\dot{z}_b - \dot{z}_w) - \frac{V}{\beta_e}\dot{P}_2 + \frac{(P_1 - P_2)}{R_i} \tag{24}$$

The actuator hydraulic force is given by

$$F = A(P_1 - P_2) \tag{25}$$

This force is inserted into the suspension equations of motion, which are

$$M\ddot{z}_b = F\cos\alpha - B_v(\dot{z}_b - \dot{z}_w) \tag{26}$$

$$m\ddot{z}_w = -F\cos\alpha + B_v(\dot{z}_b - \dot{z}_w) + k_t(z_r - z_w) + B_t(\dot{z}_r - \dot{z}_w) \tag{27}$$

Equations (19) and (23) to (27) are then combined into state space notation, as given in equations (1) and (2) in the main text. It should be noted that by considering Laplace transformations of equations (19) and (23) to (27) and neglecting initial conditions allows

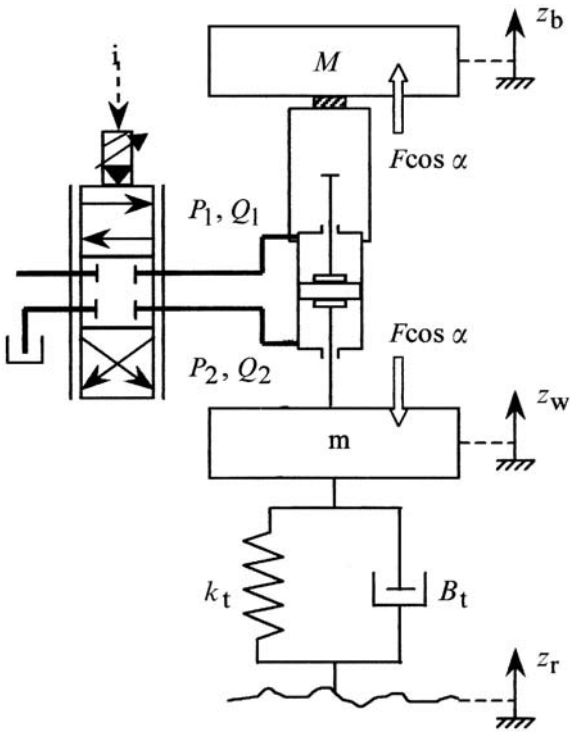

Fig. 12 Schematic of the suspension

the force transfer function to be written

$$F = \frac{k_i A}{\left(\frac{sV}{2\beta_e} + \frac{1}{R_i}\right)} i - \frac{sA^2}{\left(\frac{sV}{2\beta_e} + \frac{1}{R_i}\right)}(z_b - z_w) \tag{28}$$

In reality, this force transfer function is more complex than generally used in previous studies, due to the presence of actuator leakage. The second term on the right-hand side of (27) changes from a hydraulic spring characteristic, when $R_i \to \infty$ for no leakage, to high-pass filter characteristic in the presence of leakage [**1**].